Inorg. Chem. **2004**, *43*, 3804–3811

Structure and Magnetism of a Spin Ladder System: $(C_5H_9NH_3)_2CuBr_4$

Roger D. Willett*

Department of Chemistry, Washington State University, Pullman, Washington 99164

Calin Galeriu and Christopher P. Landee

Department of Physics, Clark University, Worcester, Massachusetts 01610

Mark M. Turnbull

Carlson School of Chemistry and Biochemistry, Clark University, Worcester, Massachusetts 01610

Brendan Twamley

University Research Office, University of Idaho, Moscow, Idaho 83844

Received November 12, 2003

The crystal structure of bis(cyclopentylammonium)tetrabromocuprate(II) has been determined at room temperature and at −70 °C. The room temperature structure is orthorhombic, space group $Pn2_1a$, with $a = 12.092(6)$ Å, $b = 8.134(4)$ Å, and $c = 18.698(10)$ Å. The low temperature structure is also orthorhombic, space group $Pna2_1$, with $a = 24.111(5)$ Å, $b = 8.089(2)$ Å, and $c = 18.448(4)$ Å. DSC studies reveal the presence of a weak endotherm at −13 °C. The structures of the two phases are very similar, differing only in the relative orientations of the cyclopentyl rings of the organic cations and slight displacements of the anionic tetrahedra. The $CuBr_4^{2-}$ anions in the low temperature phase are arranged to define a spin ladder system through Cu–Br···Br–Cu two-halide exchange pathways. Magnetic susceptibility data have been analyzed and yield antiferromagnetic exchange strengths $2J_{rail}/k = -11.6$ K and $2J_{rung}/k = -5.5$ K with a singlet–triplet gap energy $\Delta/k_B = 2.3$ K. This is the first report of a spin ladder with a stronger interaction along the axis of the ladder than along the rungs.

Introduction

Copper(II) halides have had a long and colorful history of producing significant and novel spin-$^1/_2$ Heisenberg magnetic systems. These include a series of structures with two-dimensional ferromagnetic interactions based on the $(RNH_3)_2CuX_4$ layer perovskite structures,[1] the first examples of systems with one-dimensional ferromagnetic interactions,[2] as well as systems which exhibit one- and two-dimensional antiferromagnetic behavior.[2c,3] The exchange coupling in all these systems involves single halide Cu−X−Cu pathways, and the study of the magneto-structural correlations in such pathways has been a major area of activity in the past several decades. Because of the structural flexibility of the copper(II) halide coordination sphere and of the Cu−X−Cu linkages, a seemingly endless plethora of spin-$^1/_2$ Heisenberg systems has been investigated. The interest in complex magnetic systems, such as spin ladders, alternating exchange chains, and frustrated systems has led to a renewed interest

* To whom correspondence should be addressed. E-mail: rdw@mail.wsu.edu.

(1) (a) De Jongh, L. J.; Miedema, A. R. *Adv. Phys.* **1974**, *23*, 1. Steadman, J. P.; Willett, R. D. *Inorg. Chim. Acta* **1970**, *4*, 367. (b) Barendregt, F.; Schenk, H. *Physica* **1970**, *49*, 465. (c) Willett, R. D. *Acta Crystallogr.* **1990**, *C46*, 565. (d) Tichy, K.; Benes, J.; Holg, W.; Arend, H. *Acta Crystallogr.* **1978**, *B34*, 2970. (e) Middleton, M.; Place, H.; Willett, R. D. *J. Am. Chem. Soc.* **1988**, *110*, 8639. (f) Landee, C. P.; Halvorson, K.; Willett, R. D. *J. Appl. Phys.* **1987**, *61*, 3295.

(2) (a) Willett, R. D.; Landee, C.; Swank, D. D. *J. Appl. Phys.* **1978**, *49*, 1329. (b). Swank, D. D.; Landee, C. P.; Willett, R. D. *Phys. Rev. B* **1979**, *20*, 2154. (c) Landee, C. P.; Willett, R. D. *Phys. Rev. Lett.* **1979**, *43*, 463. (d) Willett, R. D.; Landee, C. P.; Gaura, R. M.; Swank, D. D.; Groenendijk, H.; van Duyneveldt, A. J. *J. Magn. Magn. Mater.* **1980**, *15−18*, 1055. (e) Landee, C. P.; Willett, R. D. *J Appl. Phys.* **1981**, *52*, 2240. (f) Landee, C. P.; Willett, R. D. *J. Phys.* **1978**, *39*, 741.

(3) (a) Woodward, F. M.; Albrecht, A. S.; Wynn, C. M.; Landee, C. P.; Turnbull, M. M. *Phys. Rev. B* **2002**, *65*, 144412−1−13. (b) Woodward, F. M.; Landee, C. P.; Giantsidis, J.; Turnbull, M. M.; Richardson, C. *Inorg. Chim. Acta* **2001** *324*, 324.

10.1021/ic030317a CCC: $27.50
Published on Web 04/08/2004

in the study of the magnetic behavior of copper(II) halide compounds.

More recently, it has been realized that significant antiferromagnetic exchange coupling may occur through so-called two-halide (2X) exchange pathways that involve contacts between halide ions on neighboring copper(II) centers. This is most clearly demonstrated for the diammonium layer perovskite series $(NH_3RNH_3)CuX_4$ where antiferromagnetic coupling between the eclipsed ferromagnetic perovskite layers increases exponentially as the length of the diammonium cation (and thus the interlayer X···X distance) decreases.[4] In fact, for the $(NH_3C_2H_4NH_3)CuBr_4$ system, the magnitude of the interlayer coupling is larger than the intralayer coupling. The reason for the existence of significant 2X coupling in copper(II) halide systems can be easily understood from the analysis of EPR data on these systems, which show that the unpaired electron density is significantly delocalized from the Cu d orbitals into the σ ligand orbitals.[5] This delocalization is exceptionally large because of the near match in energies for the Cu d orbitals and the ligand HOMOs. Since this energy difference is less for X = Br than for X = Cl, the delocalization is greater for the bromide salts, and thus, the role of the 2X exchange is expected (and observed) to be greater for the bromide systems.

The existence of these 2X exchange pathways has been utilized to study a variety of magnetic systems, which have previously been inaccessible experimentally.[6] A series of compounds based on the C-centered monoclinic (5-X-2-aminopyridinium)$_2CuBr_4$ structure (X = Cl, Br or methyl) gives rise to a two-dimensional square lattice with antiferromagnetic coupling.[3,7] The exchange constants are such ($|J/k| \sim 6-10$ K) that the critical fields are sufficiently low ($H_c < 30$ T) that the field dependent behavior can be conveniently investigated. Similarly, a variety of ladder systems have been generated with varying rations of J_{rung}/J_{rail}.[8]

The magnetic model of a spin ladder is relatively recent.[9] Such ladders consist of two parallel chains with intrachain exchange strengths, J_{rail}, which are linked to each other by a second interaction, J_{rung}. The most interesting case occurs when both interactions are antiferromagnetic. Interest in the physics community grew after it was realized that the ground state was a spin singlet induced by and proportional to J_{rung}, no matter how large the ratio J_{rail}/J_{rung}. Further studies[9c] predicted that spin ladders with mobile charge carriers could become superconducting, a prediction confirmed in several copper oxide spin ladders.[9d,e]

Application of an external magnetic field will close the singlet−triplet gap, Δ, and induce a moment in the ladder when the Zeeman energy exceeds the gap energy. The gap will close at the lower critical field H_{C1} while a second critical field, H_{C2}, will bring all moments in alignment with the field, with the critical fields proportional to the exchange strengths. No critical fields have been observed for the oxide spin ladders due to the large exchange strengths mediated by superexchange through the oxide ions, since $J_{rail} \approx J_{rung} \approx 1000$ K. Critical fields for spin ladders have only been observed for molecular-based ladder systems with exchange strengths on the order of tens of Kelvin.[8]

In our continuing study of the structural and magnetic behavior of copper(II) halide systems, we report in this paper the properties of the compound $(CPA)_2CuBr_4$ (where CPA^+ is the cyclopentylammonium cation). This compound exists in two closely related crystalline forms, and the inter-relation of the two structures will be described. The Br···Br contacts in the low temperature structure define a spin ladder system, and the analysis of the magnetic data will be presented.

Experimental Section

Crystals of $(CPA)_2CuBr_4$ were grown by evaporation of an aqueous solution containing a 2:1 ratio of (CPA)Br and $CuBr_2$. A few drops of HBr were added to the solution to avoid hydrolysis of the Cu(II) ion. DSC measurements, made in the temperature range −140 to 40 °C with a Perkin-Elmer DSC-7 instrument, revealed the existence of a weak endotherm at −13 °C with $\Delta H = 0.56$ J/g.

X-ray Diffraction. Crystals were attached to a glass fiber using glue. Two datasets were collected at 297(2) and 203(2) K, respectively, using a Bruker/Siemens SMART 1K instrument (Mo Kα radiation, $\lambda = 0.71073$ Å) equipped with a Siemens LT-2A low temperature device. Data for both temperatures were measured using ω scans of 0.3° per frame for 30 s, and a half sphere of data was collected. A total of 1471 frames were collected with a final resolution of 0.9 Å for room temperature data and 0.84 Å for the low temperature data. The first 50 frames were re-collected at the end of data collection to monitor for decay. Cell parameters were retrieved using SMART[10] software and refined using SAINTPlus[11] on all observed reflections. Data reduction and correction for Lp and decay were performed using the SAINTPlus software. Absorp-

(4) (a) Halvorson, K.; Willett, R. D. *Acta Crystallogr.* **1988**, *C44*, 2071. (b) Block, R.; Jansen, L. *Phys. Rev. B* **1982**, *26*, 148. (c) Rubenacker, G. V.; Waplak, S.; Hutton, S. L.; Haines, D. N.; Drumheller, J. E. *J. Appl. Phys.* **1985**, 57, 3341. (d) Snively, L. O.; Haines, D. N.; Emerson, K.; Drumheller, J. E. *Phys. Rev. B* **1982**, *26*, 5245. (e) Snively, L. O.; Seifert, P. L.; Emerson, K.; Drumheller, J. E. *Phys. Rev. B* **1979**, *20*, 2101. (f) Snively, L. O.; Tuthill, G.; Drumheller, J. E. *Phys. Rev. B* **1981**, *24*, 5349.

(5) Chow, C.; Willett, R. D. *J. Chem. Phys.* **1973**, *59*, 2620

(6) (a) Patyal, B R.; Scott, B.; Willett, R. D. *Phys. Rev. B* **1990**, *41*, 1657. (b) Zhou, P.; Drumheller, J. E.; Rubenacker, G. V.; Halvorson, K.; Willett, R. D. *J. Appl. Phys.* **1991**, *69*, 5804.

(7) (a) Albrecht, A. S.; Landee, C. P.; Slanic, Z.; Turnbull, M. M. *Mol. Cryst. Liq. Cryst.* **1997**, *305*, 333. (b) Turnbull, M. M.; Albrecht, A. S.; Jameson, G. B.; Landee, C. P. *Mol. Cryst. Liq. Cryst.* **1999**, *335*, 245. (c) Matsumoto, T.; Miyazaki, Y.; Albrecht, A. S.; Landee, C. P.; Turnbull, M. M.; Sorai, M. *J. Phys. Chem. B* **2000**, *104*, 9993.

(8) (a) Luque, A.; Sertucha, J.; Lezama, L.; Rojo, T.; Roman, P. *J. Chem. Soc., Dalton Trans.* **1997**, 847. (b) Watson, B. C.; Kotov, V. N.; Meisel, M. W.; Hall, D. W.; Granoth, G. E.; Montfrooij, W. T.; Nagnler, S. E.; Jensen, D. A.; Backov, R.; Petruska, M. A.; Fanucci, G. E., Talham, D. R. *Phys. Rev. Lett.* **2001**, *86*, 5168. (c) Landee, C. P.; Turnbull, M. M.; Galeriu, C.; Giantsidis, J.; Woodward, F. M. *Phys. Rev. B* **2001**, *63*, 100402R. (d) Turnbull, M. M.; Galeriu, C.; Giantsidis, J.; Landee, C. P. *Mol. Cryst. Liq. Cryst.* **2002**, *376*, 469.

(9) (a) Dagotto, E.; Rice, T. M. *Science* **1996**, *271*, 618. (b) Dagotto, E.; *Rep. Prog. Phys.* **1999**, *62*, 1525. (c) Barnes, T.; Dagotto, E.; Riera, J.; Swanson, E. S. *Phys. Rev. B* **1993**, *47*, 3196. (d) Dagotto, E.; Riera, J.; Scalapino, D. J. *Phys. Rev. B* **1992**, *45*, 5744. (e) Nagato, T.; Uehara, M.; Goto, J.; Akimitsu, J. Motoyama, N.; Eisaki, H.; Uchida, S.; Takahashi, H.; Nakanishi, T.; Mori, N. *Phys. Rev. Lett.* **1998**, *81*, 1090. (f) Dhalenne, A.; Revcolevschi, R. *Science* **1998**, *279*, 345.

(10) *SMART: Bruker Molecular Analysis Research Tool*, v.5.059; Bruker AXS: Madison, WI, 1997−98.

(11) *SAINTPlus: Data Reduction and Correction Program*; Bruker AXS: Madison, WI, 1999.

Table 1. Crystal Data and Structure Refinement Parameters

empirical formula	$C_{10}H_{24}Br_4CuN_2$	$C_{10}H_{24}Br_4CuN_2$
fw	555.49	555.49
T (K)	297(2)	203(2)
λ (Å)	0.71073	0.71073
cryst syst	orthorhombic	orthorhombic
space group	$Pn2_1a$	$Pna2_1$
a (Å)	12.090(6)	24.111(5)
b (Å)	8.130(4)	8.0886(16)
c (Å)	18.685(10)	18.448(4)
V (Å^3)	1836.6(16)	3597.8(12)
Z	4	8
ρ_{calcd} (Mg/m^3)	2.009	2.051
μ (mm^{-1})	9.877	10.084
F(000)	1068	2136
cryst size (mm^3)	0.20 × 0.19 × 0.04	0.20 × 0.19 × 0.04
indep reflns	2618 [R(int) = 0.0653]	6173 [R(int) = 0.0785]
%T (max and min)	0.693, 0.242	0.688, 0.238
GOF on F^2	1.033	1.017
R1 ($I > 2\sigma$)[a]	0.0670	0.0603
wR2 ($I > 2\sigma$)[b]	0.1667	0.1180

[a] $R1 = \sum||F_o| - |F_c||/\sum|F_o|^2$. [b] $wR2 = \{\sum[w(F_o^2 - F_c^2)\sum/\sum[w(F_c^2)^2]\}^{1/2}$.

tion corrections were applied using SADABS.[12a] The structures were solved by direct methods and refined by least-squares method on F^2 using the SHELXTL program package.[12b] The structures of both forms were solved in the space group $Pna2_1$ by analysis of systematic absences, although the parameters for the room temperature structure were later transformed to the nonstandard $Pn2_1a$ setting for easier comparison of the two structures. The room temperature data displayed high libration with poor data leading to the lower resolution of 0.9 Å. Attempts at modeling the cyclopentylammonium rings as disordered were not successful, and the model shown was kept. The C−C bond lengths and angles were constrained due to the high libration. All non-hydrogen atoms were refined anisotropically. The low temperature structure is closely related to that of the room temperature structure, but it has a doubled a-axis and $Z = 8$. One of the four crystallographically independent cyclopentylammonium rings was disordered and modeled with occupancies of 45% and 55% for each moiety. The other cations had very large U_{eq} values and likely exhibited torsional disorder of the cyclopentyl rings. Most of the C−C distances were constrained. Hydrogen atom positions were calculated and added geometrically for both refinements with a riding model, their parameters constrained to the parent atom site. No decomposition was observed during data collection. Details of the data collection and refinement are given in Table 1. Positional parameters and U_{eq} values are given in Tables 2 and 3 while Table 4 summarizes the bond distances and angles for the $CuBr_4^{2-}$ anions. The asymmetric units of the two structures are illustrated in Figure 1a,b for the room and low temperature structures, respectively. Further details are provided in the Supporting Information.

Magnetic Studies. The susceptibility study was done on crushed single crystal samples using a Quantum Design MPMS SQUID magnetometer. The magnetization of the sample was first determined as a function of field at 2 K and found to be linear up to 2 T. No hysteresis was detected. For the determination of the molar magnetic susceptibility χ_{mol}, the magnetic moment of the compound was determined in a field of 1 T as a function of temperature between 2.0 and 300 K. Corrections to the molar susceptibility have been made for the temperature independent magnetization of the Cu(II) ion (60×10^{-6} emu/mol), and the diamagnetic contribution was calculated from Pascal's constants (-290×10^{-6} emu/mol). A room temperature measurement of a powder sample on a Bruker

(12) (a) Sheldrick, G. M. *SADABS v.2.01: an empirical absorption correction program*; Bruker AXS Inc.: Madison, WI, 1999. (b) Sheldrick, G. M. *SHELXTL: Structure Determination Software Suite*, version 5.10; Bruker AXS Inc.: Madison, WI, 1998.

Table 2. Atomic Coordinates ($\times 10^4$) and Equivalent Isotropic Displacement Parameters (Å$^2 \times 10^3$) for the Room Temperature Structure

atom	x	y	z	U(eq)
Cu	2472(1)	3656(8)	4560(1)	75(1)
Br(1)	4384(1)	3623(10)	4305(1)	114(1)
Br(2)	1925(3)	6261(2)	4118(3)	121(2)
Br(3)	1880(3)	1090(2)	4115(4)	116(2)
Br(4)	1427(2)	3675(11)	5622(1)	128(1)
N(1)	−805(11)	3940(40)	4520(8)	130(9)
C(1)	−1253(15)	3370(50)	3921(10)	159(11)
C(2)	−791(16)	3610(60)	3257(11)	172(10)
C(3)	−1750(20)	4080(60)	2775(12)	190(12)
C(4)	−2665(17)	3400(80)	3107(14)	191(12)
C(5)	−2436(14)	3360(70)	3861(11)	171(12)
N(11)	5778(12)	3510(50)	5828(8)	134(8)
C(11)	5040(30)	4060(50)	6364(12)	219(12)
C(12)	4280(20)	2800(40)	6530(13)	196(13)
C(13)	4150(30)	2740(40)	7272(14)	233(14)
C(14)	5010(30)	3720(70)	7576(11)	245(12)
C(15)	5510(30)	4580(40)	7024(14)	213(13)

[a] U(eq) is defined as one-third of the trace of the orthogonalized U_{ij} tensor.

Table 3. Atomic Coordinates ($\times 10^4$) and Equivalent Isotropic Displacement Parameters (Å$^2 \times 10^3$) for the Low Temperature Structure[a]

atom	x	y	z	U(eq)
Cu(1)	4915(1)	12064(2)	2223(3)	40(1)
Cu(2)	2443(1)	8118(2)	3175(3)	36(1)
Br(1)	4736(1)	9475(2)	1684(3)	68(1)
Br(2)	4399(1)	11733(2)	3300(2)	51(1)
Br(3)	4559(1)	14707(1)	1861(2)	47(1)
Br(4)	5875(1)	12436(2)	1974(3)	57(1)
Br(5)	2797(1)	5483(1)	3532(2)	44(1)
Br(6)	1482(1)	7680(2)	3430(2)	51(1)
Br(7)	2580(1)	10745(2)	3702(2)	53(1)
Br(8)	2972(1)	8488(2)	2106(3)	50(1)
N(1)	3289(4)	12717(14)	2269(8)	50(4)
N(2)	4073(5)	7492(13)	3119(9)	53(4)
N(3)	6492(5)	11574(14)	3552(7)	55(4)
N(4)	782(5)	8223(15)	1881(7)	62(4)
C(1)	3026(7)	13437(18)	1620(9)	53(4)
C(2)	3235(8)	12690(20)	897(13)	80(6)
C(3)	2757(8)	12600(40)	433(14)	120(9)
C(4)	2240(9)	12880(40)	874(11)	147(12)
C(5)	2399(6)	13160(20)	1641(10)	74(6)
C(6)	4308(6)	6837(17)	3804(11)	61(5)
C(7)	4929(7)	7070(20)	3873(14)	82(6)
C(8)	5063(10)	7310(30)	4646(17)	120(10)
C(9)	4593(11)	8400(30)	4879(13)	123(10)
C(10)	4094(7)	7790(20)	4474(9)	61(5)
C(11)	6047(7)	11457(14)	4113(8)	50(4)
C(12)	6251(10)	10950(20)	4814(13)	114(8)
C(13)	6410(10)	12490(30)	5219(14)	136(11)
C(14)	6008(11)	13770(20)	4934(11)	121(9)
C(15)	5812(7)	13125(19)	4224(8)	67(5)
C(16A)	1203(7)	8490(50)	1331(12)	80(6)
C(17A)	959(12)	8770(40)	564(13)	80(6)
C(18A)	1316(11)	7660(40)	64(17)	80(6)
C(19A)	1881(11)	8150(50)	401(8)	80(6)
C(20A)	1839(6)	8300(30)	1237(8)	80(6)
C(16B)	1022(6)	7550(30)	1225(8)	97(6)
C(17B)	839(6)	7880(30)	432(8)	97(6)
C(18B)	1387(9)	8350(40)	46(17)	97(6)
C(19B)	1756(13)	7010(40)	398(15)	97(6)
C(20B)	1623(8)	6870(40)	1217(15)	97(6)

[a] U(eq) is defined as one-third of the trace of the orthogonalized U_{ij} tensor.

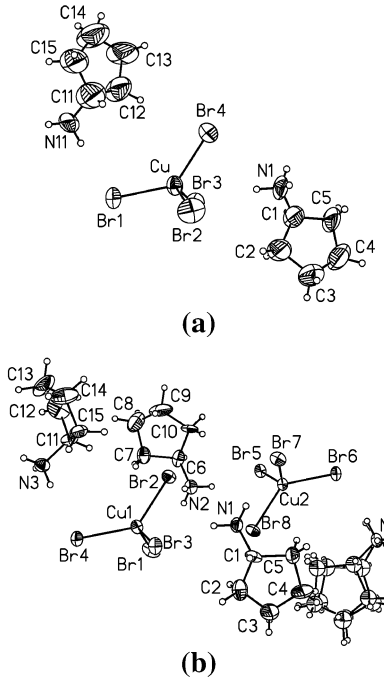

Figure 1. Thermal ellipsoid illustrations of the asymmetric units of (a, upper) the room temperature structure and (b, lower) the low temperature structure. Ellipsoids shown at 30% level.

Table 4. Bond Lengths [Å] and Angles [deg]

room temperature		low temperature	
Cu−Br(4)	2.353(3)	Cu(1)−Br(1)	2.358(2)
Cu−Br(3)	2.357(7)	Cu(1)−Br(2)	2.359(2)
Cu−Br(1)	2.360(2)	Cu(1)−Br(4)	2.378(2)
Cu−Br(2)	2.367(6)	Cu(1)−Br(3)	2.398(2)
Br(4)−Cu−Br(3)	98.1(3)	Cu(2)−Br(7)	2.360(2)
Br(4)−Cu−Br(1)	134.1(1)	Cu(2)−Br(8)	2.368(2)
Br(3)−Cu−Br(1)	102.5(2)	Cu(2)−Br(5)	2.388(2)
Br(4)−Cu−Br(2)	98.0(2)	Cu(2)−Br(6)	2.389(2)
Br(3)−Cu−Br(2)	125.7(1)	Br(1)−Cu(1)−Br(2)	99.06(8)
Br(1)−Cu−Br(2)	102.3(2)	Br(1)−Cu(1)−Br(4)	102.08(9)
		Br(2)−Cu(1)−Br(4)	133.61(10)
		Br(1)−Cu(1)−Br(3)	127.50(10)
		Br(2)−Cu(1)−Br(3)	98.45(8)
		Br(4)−Cu(1)−Br(3)	100.48(8)
		Br(7)−Cu(2)−Br(8)	98.81(7)
		Br(7)−Cu(2)−Br(5)	129.75(9)
		Br(8)−Cu(2)−Br(5)	98.62(7)
		Br(7)−Cu(2)−Br(6)	100.87(8)
		Br(8)−Cu(2)−Br(6)	134.83(10)
		Br(5)−Cu(2)−Br(6)	99.23(7)

EMX EPR spectrometer operating at 9.3 GHz gave a Landé factor $g_{av} = 2.17$.

The low temperature magnetization was determined in fields up to 30 T using a Lake Shore model 735 vibrating sample magnetometer and a ^{4}He cryostat with a ^{3}He insert at the National High Magnetic Field Laboratory in Tallahassee, FL. The absolute accuracy of these measurements is better than 6−8% for small moments, but the relative accuracy is several orders of magnitude better. Temperatures were determined from the relevant vapor pressure scale. Both the susceptibility and magnetization studies were carried out on samples from the same batch.

Structural Description

The closely related crystal structures of the two phases consist of layers of isolated $CuBr_4^{2-}$ anions hydrogen bonded by CPA^+ cations. Both structures can be traced back to a common *Pnma* parent structure. Examination of the lattice constants show that $b_l \sim b_r$ and $c_l \sim c_r$ but $a_l \sim 2a_r$, where the l and r subscripts denote the low (−70 °C) and room (24 °C) temperature structures, respectively. The changes that occur in the phase transition involve subtle reorientation of the $CuBr_4^{2-}$ anions and the CPA^+ cations. The N−H···Br hydrogen bonding provides stability to the lattice, leading to the formation of cation/anion/cation layers lying parallel to the *ab* plane. These layers are illustrated in Figure 2a,b for the room temperature and low temperature structures, respectively, where the close relation between the two structures is apparent. In the room temperature phase, the planes of the cyclopentyl rings lie roughly perpendicular to the *b*-axis. However, in the low temperature phase, the planes of the cyclopentyl rings of one-quarter of the cations are rotated so their normals lie approximately in the *ac* plane. In the room temperature phase, both cations exhibit disorder (presumably dynamic), as evidenced by the large U_{eq} values of the carbon atoms in the cyclopentyl rings as well as the near planarity of the rings. One of the four independent cations in the low temperature phase exhibits disorder, likely due to irreversible processes occurring as the crystal passed through the phase transition. In addition, as noted above, the other three cations show evidence of librational disorder.

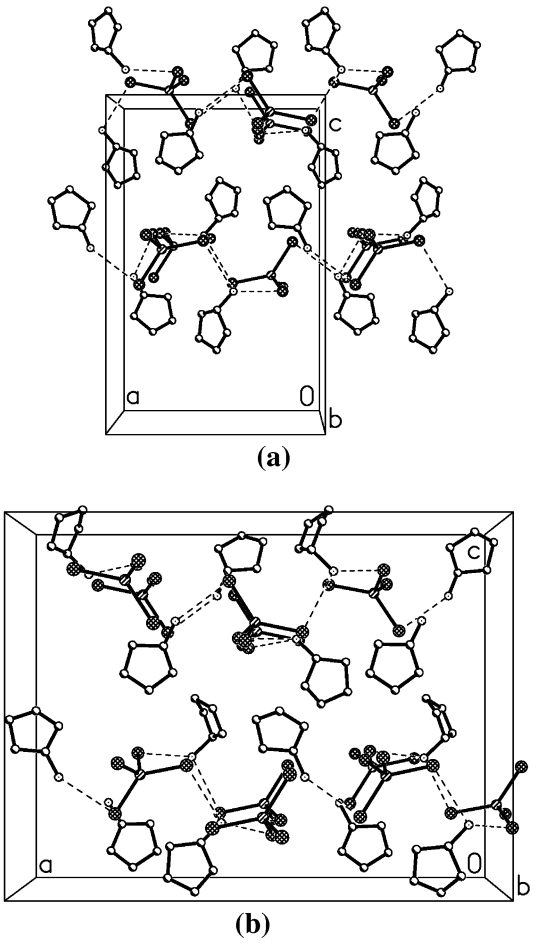

Figure 2. Illustrations of the packing of the cation/anion/cation layers (a, upper) in the room temperature structure and (b, lower) the low temperature structure. The shortest hydrogen bonds are shown by dashed lines. The views are from the *b* direction, with the *a* axis being horizontal.

Table 5. Structural Parameters for Br···Br Contacts

atoms	$\theta_{Cu-Br\cdots Br(deg)}$	$d_{Br\cdots Br(Å)}$	$\theta_{Br\cdots Br-Cu(deg)}$	$\tau_{Cu-Br\cdots Br-Cu(deg)}$
		Room Temperature Phase		
CuA−Br2A···Br3B−CuB	154.0	3.926	151.7	4.3
CuA−Br2A···Br4E−CuE	126.9	4.529	124.6	41.7
CuA−Br4A···Br3E−CuE	125.1	4.481	128.3	−41.0
		Low Temperature Phase		
Cu1A−Br1A···Br8C−Cu2C	105.3	4.396	133.8	−62.5
Cu1A−Br2A···Br7C−Cu2C	132.1	4.519	103.2	63.4
Cu1A−Br3A···Br1B−Cu1B	150.1	3.893	149.8	−55.9
Cu2C−Br7C···Br5A−Cu2A	151.0	3.881	148.8	64.3

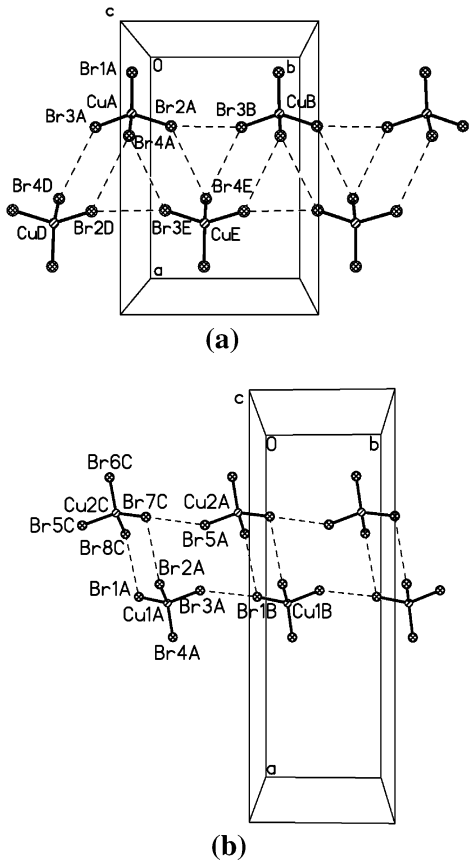

Figure 3. Illustrations of the ladder chains in (a, upper) the room temperature and (b, lower) the low temperature structures.

Details of the hydrogen bonding interactions are available as Supporting Information.

Of importance for the interpretation of the magnetic data are the Cu−Br···Br−Cu interactions within the layers described above, including the Br···Br distance (d), the Cu−Br···Br angles (θ), and the Cu−Br···Br−Cu dihedral angles (τ) (see Table 5 for details). In both phases, the shortest Br···Br contacts define double chain arrangements, with chains running parallel to the b axes. This is illustrated in Figure 3a,b for the room and low temperature phases, respectively. The shortest Br···Br contacts are between $CuBr_4^{2-}$ anions along the rails (3.926 Å for the room temperature phase (Br2A···Br3B) and 3.893 Å (Br3A···Br1B) and 3.881 Å (Br7C···Br5A), respectively, for the two independent rails in the low temperature phase). In the room temperature phase, the $CuBr_4^{2-}$ anions are arranged so that the Br···Br contacts between the rails define an ideal zigzag conformation with equal diagonal rungs (Scheme 1a). Each

Scheme 1

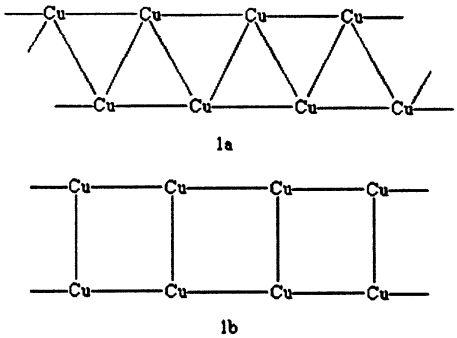

rung contains two Br···Br contacts of 4.481 and 4.529 Å. In the low temperature phase, the $CuBr_4^{2-}$ anions rotate slightly, and the two rails are displaced relative to each other parallel to the chain direction. This leads to the ladderlike configuration (Scheme 1b) shown in Figure 3b. The rung Br···Br contacts are now 4.396 Å (Br1A···Br8C) and 4.519 Å (Br2A···Br7C). The shortest diagonal contact in the ladder is 4.930 Å for Br4A···Br6C. The shortest interladder contacts are 5.049 Å in the room temperature phase (Br1···Br1, twice), while the shortest interladder contacts in the low temperature phase are 4.996 and 5.147 Å (for two different Br4···Br6 contacts).

As indicated earlier, the parent structure of both phases has symmetry *Pnma*. In this hypothetical structure, both the $CuBr_4^{2-}$ anions and the CPA^+ cations would have to lie on mirror planes. For the anions, this is feasible. However, with the cyclopentyl group of the CPA^+ cations lying parallel to the mirror plane, the CPA^+ cations cannot take an ordered conformation on the mirror planes. In the room temperature phase, the CPA^+ cations are accommodated by the simple loss of the mirror planes perpendicular to the b axis, yielding the "translationengleiche" subgroup $Pn2_1a$. However, the low temperature space group is derived by a more complex two-step route, first then losing the a-glide perpendicular to the c axis to yield the group $Pnm2_1$, then doubling the a axis to yield the "klassengleiche" group $Pna2_1$. Thus, the transition is not likely a second order phase transition, since there is not a simple group/subgroup relation between the two phases.

Magnetic Analysis

The magnetic susceptibility of $(CPA)_2CuBr_4$ between 2 and 100 K is shown in Figure 4, with the data below 20 K shown within the insert. The behavior is dominated by a rounded maximum near 8 K and a rapid decrease at lower temperatures. Such behavior is characteristic of low-

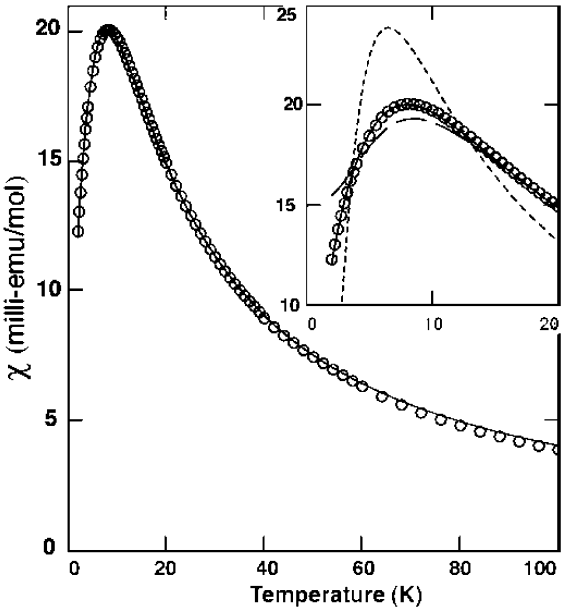

Figure 4. Magnetic susceptibility of $(CPA)_2CuBr_4$. The solid line corresponds to the spin ladder fit with the parameters $2J_{rail}/k = -11.6$ K and $2J_{rung}/k = -5.5$ K. In the inset, the dashed and dotted lines correspond to the fits to the linear chain and dimer models, respectively, as described in the text.

dimensional $S = {}^1/_2$ systems with antiferromagnetic Heisenberg exchange interactions. The higher temperature data ($T > 20$ K) are well represented by the Curie−Weiss equation with a small negative intercept on the temperature axis (Curie−Weiss parameters $C = 0.423$ emu-K/mol and $\theta = -7.3$ K). This Curie constant for low temperature phase corresponds to a *g*-factor of 2.12, in reasonable agreement with the room temperature value 2.17 determined for the room temperature phase. No anomaly is observed near 260 K (−13 °C) where the structural rearrangement occurs.

The first attempt to model the magnetic behavior used an expression for the susceptibility of a uniform $S={}^1/_2$ Heisenberg antiferromagnetic chain.[13] The justification for this model is the considerably shorter Br···Br contacts between $CuBr_4^{2-}$ anions along the extended axis (3.893 and 3.881 Å for the low temperature phase) compared to the corresponding rung Br···Br distances of 4.396 and 4.519 Å. Since the strength of the antiferromagnetic interaction decreases rapidly with bromine−bromine distance, it is plausible that a linear chain model would effectively describe the data. However, the one-dimensional (1D) fit is poor. When both *J* and the Curie constant are allowed to vary independently, values of $2J/k = -13.3$ K and $C = 0.438$ emu-K/mol ($g_{av} = 2.16$) are obtained, but overall agreement is unsatisfactory (dashed line in Figure 4). The model lies significantly below the data near the peak but lies above the data at lower temperatures. The 1D model predicts a finite value of the $T = 0$ susceptibility, but the data decrease rapidly at low temperatures, indicative of a singlet ground state.

The data were then compared to the theoretical prediction for an isolated antiferromagnetic dimer, described by the Bleaney−Bowers equation.[14] When *J* and *C* were allowed to vary independently, the best-fit parameters were found to be $2J/k = -10.4$ K and $C = 0.309$ emu-K/mol ($g_{av} = 1.82$). This fit, represented by the dotted line in Figure 4, produces an unphysical value for the Curie constant and has a peak which is both higher and narrower than the data. Nevertheless, this clearly shows that the interactions between the dimers are significant within this compound.

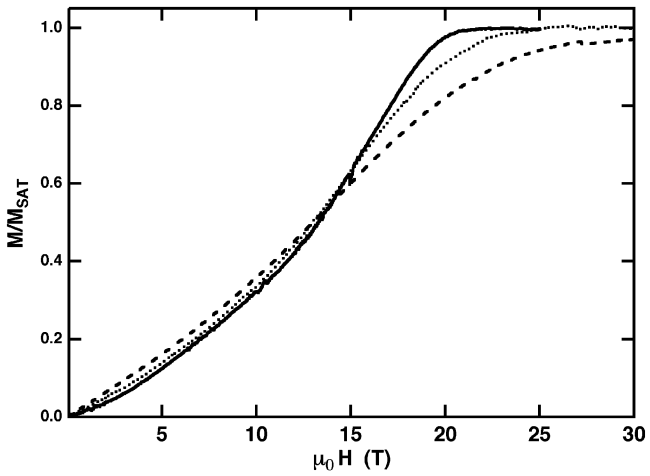

Figure 5. Relative magnetization of $(CPA)_2CuBr_4$ as a function of applied field at 0.74 K (—), 1.5 K (···), and 4.2 K (- - -).

The data were then compared to the theoretical prediction for a spin ladder, with three parameters (J_{rail}, J_{rung}, and *C*) allowed to vary independently.[15] The best fit parameters, $2J_{rail}/k_B = -11.6$ K, $2J_{rung}/k_B = -5.54$ K, and $C = 0.438$ emu-K/mol ($g_{av} = 2.16$) give an excellent agreement with the data at all temperatures (solid line in Figure 4). Both the spin ladder and linear chain fits slightly overestimate the data above 50 K (solid and dashed lines, respectively) compared to the Curie−Weiss fit which only includes data above 40 K, but the Curie constant obtained with the spin ladder fit, 0.438 emu-K/mol, is physically reasonable and within two percent of the Curie−Weiss value.

It has previously been established that the same experimental data can be fitted equally well by spin ladder or an alternating chain models;[15] the data were then compared to the theoretical prediction for an alternating chain.[13] When J_1, J_2, and *C* were allowed to vary independently, the best fit parameters were found to be $2J_1/k = -11.5$ K, $2J_2/k = -13.4$ K, and $C = 0.427$ emu-K/mol ($g_{av} = 2.13$). The predictions of this model are indistinguishable from that of the spin ladder model (solid line in Figure 4). However, the low temperature structure shows that the spin ladder is the appropriate magnetic model for this compound.

The field-dependent relative magnetization (M/M_{sat}) of a polycrystalline sample of $(CPA)_2CuBr_4$ is shown in Figure 5 for data sets collected at 0.74, 1.5, and 4.2 K. Each of the sets is characterized by a low-field linear region extending

(13) Johnston, D. C.; Kremer, R. K.; Troyer, M.; Wang, X.; Klümper, A.; Bud'ko, S. L.; Panchula, A. F.; Canfield, P. C. *Phys. Rev. B* **2000**, *61*, 9558.

(14) Bleaney, B.; Bowers, K. D. *Proc. R. Soc. London, Ser. A* **1952**, *214*, 451.

(15) Johnston, D. C.; Troyer, M.; Miyahara, S.; Lidsky, D.; Ueda, K.; Azuma, M.; Hiroi, Z.; Takano, M.; Isobe, M.; Ueda, Y.; Korotin, M. A.; Anisimov, V. I.; Mahajan, A. V.; Miller, L. L. Eprint at http://arXiv.org/abs/cond-mat/0001147.

several tesla, followed by an increasing upward curvature with an inflection point near 14 T. At higher fields the sets are marked by downward curvature until they approach or achieve saturation. The lowest temperature data set saturates by 20 T, reaching a saturation magnetization of 5650 emu/mol, a value about 6% smaller than expected for an $S = {}^1/_2$ system with $g = 2.16$. However, this discrepancy lies within the calibration uncertainty of the magnetometer used.

At $T = 0$, spin ladders are predicted to be in a cooperative singlet ground state with zero moment. Application of an external field will lower the energy of the lowest (triplet) excited state until it crosses the singlet state and becomes the new ground state at the critical field H_{c1}. At the critical field, a moment is induced discontinuously in the ladder. For finite temperatures the triplet state is thermally populated even in zero field so all magnetization curves are smooth. The derivative dM/dH can nevertheless show a maximum at H_{c1} for temperatures low compared to singlet−triplet gap Δ. A recent theoretical paper[16] predicts that the maximum in dM/dH at H_{c1} will become increasingly small as the temperature increases above $T = 0$ and vanish for temperatures greater than 13% of the gap energy. Low temperature experimental studies of other spin ladder compounds with accessible critical fields have found the magnetization anomalies corresponding to the critical fields H_{c1}: $(5IAP)_2CuBr_4 \cdot 2H_2O$, $H_{c1} = 8.3$ T;[8c] $(5NAP)_2CuBr_4 \cdot H_2O$, $H_{c1} = 7.6$ T;[8d,22] $(pipH)_2CuBr_4$, $H_{c1} = 6.6$ T.[8b] However, no maximum was observed in the dM/dH of $(CPA)_2CuBr_4$ even at the lowest experimental temperature of 0.74 K.

Knowledge of the gap energy for $(CPA)_2CuBr_4$ is necessary to understand the temperature dependence of its magnetization. The gap energy Δ can be estimated using the exchange parameters determined from the susceptibility data. Numerical calculations[17] indicate that there is a nonzero spin gap for all interchain couplings $J_{rung} < 0$ with the spin gap relatively small for $J_{rung}/J_{rail} < 0.5$. More detailed calculations[18] show that, in the region $J_{rung}/J_{rail} < 0.66$, the spin gap $\Delta = 0.41|2J_{rung}|$. For our system $J_{rung}/J_{rail} = 0.48$, and hence, $\Delta/k = 2.26$ K. Our lowest temperature of 0.74 K corresponds to 0.33Δ, well beyond the value of 0.13Δ for which the maximum of dM/dH is expected to vanish. The magnetization data are therefore consistent with the spin ladder model, but temperatures below 200 mK will be required to detect an anomaly in the magnetization.

In Figure 6, the magnetization data set of 0.74 K (—) is compared to the predictions for the magnetization curves at that temperature for a spin ladder (□) and an alternating chain (○), in each case using the set of exchange parameters obtained from the susceptibility fit to the corresponding model.[19] It is seen that the two models describe the data equally well up to about $0.6B_{sat}$, with the spin ladder model dropping below the experimental curve for higher fields and the alternating chain rising faster than the data in the same region. The disagreement between the models and the data may be due to our neglect of the fact that the magnetic exchange parameters along the rails of the ladder will not be exactly identical.

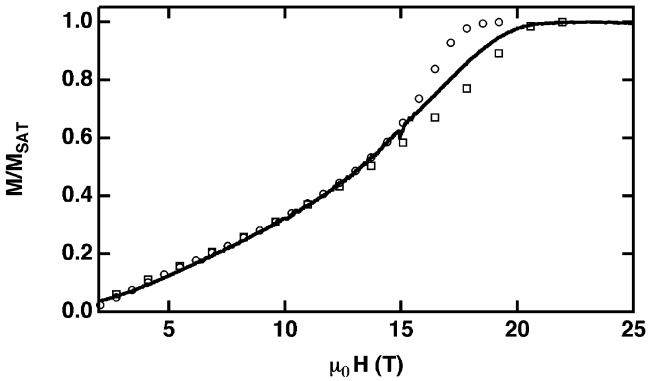

Figure 6. Comparison of the relative magnetization of $(CPA)_2CuBr_4$ at 0.74 K (—) and the results of Quantum Monte Carlo calculation for a spin ladder (□) and an alternating chain (○) using the best-fit parameters described in the text.

Magnetostructural Correlations

Numerous structural parameters affect the magnitude of the double halide exchange between $CuBr_4^{2-}$ ions. These include the bond lengths and angles at the metal center in the ion itself as well as those resulting from the packing of species in the crystal. Structural and magnetic data for a wide variety of complexes of the general form A_2CuBr_4 have been reported, and data for several of these compounds are reported in Table 6. These compounds represent a variety of packing motifs including chains,[20] ladders,[8c,d] and square lattices.[7d,e] We note that some authors have interpreted their results in terms of a superexchange pathway involving a combination of hydrogen bonding, π-stacking, and double halide interactions. We have presented the structural data as it applies to halide−halide contacts only.

It is clear from the data in Table 6 that the exchange parameters determined for $(CPA)_2CuBr_4$ (−5.5 and −11.6 K) are well within the range usually observed for double halide exchange. In cases where other structural parameters (θ, τ) are similar, there is an inverse relationship between the magnetic exchange and the nonbonding Br···Br distance (entries 5−7). However, other parameters clearly affect the exchange as well, as can be seen by comparison of entry 4 with entries 5−7, or entries 4 and 8. In these cases, entry 4 exhibits a shorter Br···Br contact distance, but also a smaller J value.

$(CPA)_2CuBr_4$ is different from other spin ladders in two ways. First, its rung interaction is only half as strong ($2J_{rung}/k = -5.5$ K) as that along the rails of the ladder ($2J_{rail}/k = -11.6$ K). The other reported copper bromide spin ladders (Table 6) either have dominant rung interactions (5IAP: −13

(16) Wang, X.; Yu, L. *Phys. Rev. Lett.* **2000**, *84*, 5399.
(17) Barnes, T.; Dagotto, E.; Riera, J.; Swanson, E. *Phys. Rev. B* **1993**, *47*, 3196.
(18) Greven, M.; Birgeneau, R. J.; Wiese, U.-J. *Phys. Rev. Lett.* **1997**, *77*, 1865.
(19) These results were obtained using an extensive Quantum Monte Carlo simulation of the magnetization of the individual models using the described parameters. We thank Professor Mathias Troyer of the ETH-Zurich for making these results available to us.
(20) Luque, A.; Sertucha, J.; Castillo, O.; Román, P. *Polyhedron* **2002**, *21*, 19.

Table 6. Structure and Magnetic Exchange Parameters for A_2CuBr_4 Compounds

	compd	lattice	pathway	$\theta_{Cu-Br\cdots Br}$	$d_{Br\cdots Br}$	$\theta_{Br\cdots Br-Cu}$	$\tau_{Cu-Br\cdots Br-Cu}$	$2J/k$ (K)	ref
1	$(CPA)_2CuBr_4$[a]	ladder	rungs	105.3	4.396	133.8	−62.5	−5.5	this work
				132.1	4.519	103.2	63.4		
			rails	150.1	3.893	149.8	−55.9	−11.6	
				151.0	3.881	148.8	64.3		
2	$(5IAP)_2CuBr_4\cdot 2H_2O$	ladder	rung	151.9	3.58	151.9	180	−13.0	8c
			rail	122.0	4.23	95	98	−1.15	
3	$(5NAP)_2CuBr_4\cdot H_2O$	ladder	rung[b]	148.6	4.067	92.3	−7.6	−20.4	8d, 22
			rail	132.5	3.931	146.5	−3.6	−19.5	
4	$(3\text{-}Etpy)_2CuBr_4$[b]	chain		109.1	4.213	151.4	3.8	−2.44	20
5	$(5MAP)_2CuBr_4$	square		133.7	4.55	143.8	16.0	−6.6	7e
6	$(5BAP)_2CuBr_4$	square		138.9	4.39	136.7	21.6	−6.94	7d
7	$(5CAP)_2CuBr_4$	square		138.9	4.30	137.0	21.9	−8.7	7e
8	$(4\text{-}Etpy)_2CuBr_4$	alternating		142.0	4.02	142.0	180	−4.32	20
		chain		136.4	4.46	136.4	180	−3.46	
9	$(pipH)_2CuBr_4$	ladder	rung[b]	133.7	4.10	115.1	47.3	−13.3	6a, 8b
			rail	146.0	4.31	153.5	53.0	−3.8	

[a] Low temperature phase. [b] Two identical contacts between $CuBr_4^{2-}$ units. CPA = cyclopentylammonium; 5IAP = 5-iodo-2-aminopyridinium; 5NAP = 5-nitro-2-aminopyridinium; 3-Etpy = 3-ethylpyridinium; 5MAP = 5-methyl-2-aminopyridinium; 5BAP = 5-bromo-2-aminopyridinium; 5CAP = 5-chloro, 2-aminopyridinium; 4-Etpy = 4-ethylpyridinium; pipH = piperidinium.

K /−1 K. pipH: −13.3/−3.8 K), or rung and rail interactions which are equivalent (5NAP: −19.5/−20.4). The non-copper bromide spin ladder $[(DT\text{-}TTF)_2][Au(mnt)_2]$ has considerably stronger exchange strengths, but once again the rung interactions dominate ($2J_{rung}/k = -142$ K; $2J_{rail}/k = -83$ K).[21] Theoretical studies have shown that ladders for which the $|J_{rung}/J_{rail}| > 2$ may be readily described with a perturbation model in which isolated $S = {}^1/_2$ dimers are weakly coupled by the rail interaction, with the triplet states being converted into a narrow band of bandwidth J_{rail}. As the ratio $|J_{rung}/J_{rail}|$ decreases, the perturbation model rapidly becomes inapplicable, and the full description of the ladder becomes a many-body problem. Although $(CPA)_2CuBr_4$ is structurally similar to the other copper bromide ladders of Table 6, its magnetic energy spectrum is expected to be greatly different.

The second difference between $(CPA)_2CuBr_4$ and the other spin ladders is that the two rails of the ladder in $(CPA)_2CuBr_4$ are not identical by symmetry. They have very similar values for the Br···Br contact distances (3.881 and 3.892 Å) and Cu−Br···Br angles θ (150.1°, 151.0°) so we do expect similar values for the two rail exchange strengths. The value reported represents the effective value for this compound.

The two Br−Br contact distances are only slightly shorter than the value of 3.931 Å seen for the rails in $(5NAP)_2CuBr_4\cdot H_2O$ (entry 3), but the effective interaction is ∼30% weaker. The θ values for the two compounds are similar (±10%), but there is a distinct difference in the τ values, with the $(5NAP)_2CuBr_4\cdot H_2O$ compound being nearly eclipsed ($\tau = -3.6°$), but $(CPA)_2CuBr_4$ being closer to gauche ($\tau \sim 60°$). It is clear from the data presented in Table 6 that additional data and extensive theoretical work will be required before complete understanding of the effects of the various structural parameters is possible.

Conclusion

$(CPA)_2CuBr_4$ has been shown to undergo a first order structural transition near −13 °C to a low temperature structure corresponding to a spin ladder packing of the $CuBr_4^{2-}$ anions. Magnetic studies of the low temperature phase indicate that the coupling down the rails of the ladder (−11.6 K) is considerably stronger than the exchange strength across the rungs (−5.5 K). This is the first known spin ladder with dominant rail interactions. The exchange strengths of $(CPA)_2CuBr_4$ are typical of those found for other lattices of packed $CuBr_4^{2-}$ anions, but there is not yet a clear set of correlations between structural parameters and strength of magnetic interactions.

Acknowledgment. The Bruker (Siemens) SMART APEX diffraction facility was established at the University of Idaho with the assistance of the NSF-EPSCoR program and the M. J. Murdock Charitable Trust, Vancouver, WA. Work was supported in part by ACS-PRF 34779-AC. The Clark University group thanks Professor Joe Budnick (University of Connecticut) for the use of his SQUID magnetometer. A portion of this work was performed at the National High Magnetic Field Laboratory, which is supported by NSF Cooperative Agreement DMR-0084173 and by the State of Florida. The authors appreciate the assistance of Braunen Smith with the figures.

Supporting Information Available: Crystal data in CIF format. This material is available free of charge via the Internet at http://pubs.acs.org.

IC030317A

(21) Rovira, C.; Veciana, J.; Ribera, E.; Tarrés, J.; Canadell, E.; Rousseau, R.; Mas, M.; Molins, E.; Almeida, M. Henriques, R. T.; Morgado, J.; Schoeffel, J.-P.; Pouget, J.-P. *Angew. Chem., Int. Ed. Engl.* **1997**, *36*, 2324.

(22) Galeriu, C. M.A. Thesis, Clark University, 2002.